J Mater Sci (2008) 43:1576–1582
DOI 10.1007/s10853-007-2330-2

Adiabatic shear band in a Ti-3Al-5Mo-4.5V Titanium alloy

B. F. Wang

Received: 13 February 2007 / Accepted: 19 November 2007 / Published online: 31 December 2007

Abstract An investigation has been carried out on the adiabatic shear band (ASB) in a Ti-3Al-5Mo-4.5V (TC16) alloy deformed at high strain rate by a split Hopkinson pressure bar (SHPB). ASB in TC16 alloy is a "white" band with a width of about 13 μm. Microhardness of the ASB is larger than that of the matrix. The elongated cell structures of width about 0.2–0.5 μm with thick dislocation exist in the boundary of the shear band. Results suggest that the fine equiaxed grains with α-phase and α″-phase coexist in the shear band. The "white" band is a transformation band. Calculation of the adiabatic temperature rise indicates that the maximum temperature within ASB is about 1,069 K that is above the phase transformation temperature. Finally, formation of an ASB in the TC16 alloy and its microstructure evolution are described.

Introduction

Adiabatic shear banding is an important thermoviscoplastic instability mode observed in metals when processed at high strain rates [1]. Due to the properties of low heat conductivity and high adiabatic shearing sensitivity, adiabatic shear band (ASB) is easily observed in titanium and its alloys [2–4]. Ti-3Al-5Mo-4.5V (TC16) alloy is a kind of martensite strengthening ($\alpha + \beta$) titanium alloy with good mechanical and processing properties, such as hot deformability, weldability, machine workability, and corrosion resistance, and it has wide application in the aerospace industry [5]. Many researches had been carried out in the study of the conventional processing of Ti-Al-Mo-V alloy [6–9]. However, there are few reports about the high-velocity shear deformation of the TC16 alloy, especially the report of ASB in it.

The objectives of this paper are to report observations of the microstructure in ASB in TC16 alloy and to discuss the formation of ASB and to calculate the thermal–mechanical parameters in ASB during the deformation.

Experimental

The composition (wt.%) of the TC16 alloy was: Al 3%, Mo 5%, V 4.5%, Ti constituting the remaining. The alloy was previously cold worked and received as a cylinder with a diameter of 20 mm and a length of 200 mm.

The hat-shaped specimen, originally developed by Meyer and Manwarig [10], was used to produce ASBs in TC16 alloy at a high strain rate under adiabatic conditions. The specimen was dynamically compressed using a split Hopkinson pressure bar (SHPB).

From the results of Andrade and Meyers [11], the shear stress (τ), strain (γ), and strain rate ($\dot{\gamma}$) in the shear band were expressed as Eqs. 1, 2, and 3, respectively. Culver [12] introduced a simple relation between the true strain (ε) and the shear strain (γ) expressed as Eq. 4.

$$\tau(t) = \frac{E_0 d_i^2 e_t(t)}{L(d_i + d_e)} \tag{1}$$

$$\dot{\gamma} = \frac{2C_0 e_r(t)}{W} \tag{2}$$

B. F. Wang (✉)
School of Materials Science and Engineering, Central South University, Changsha 410083, Hunan,
People's Republic of China
e-mail: bingfeng_wang@yahoo.com.cn

$$\gamma = \int_0^t \dot{\gamma}\, \mathrm{d}t \tag{3}$$

$$\varepsilon = \ln\sqrt{1+\gamma+\frac{\gamma^2}{2}} \tag{4}$$

where E_0 and C_0 were the elastic modulus and elastic wave speed in SHPB, $e_r(t)$ and $e_t(t)$ shown in Fig. 1 were experimentally measured strains of reflected and transmitted stress pulse on the Hopkinson bars, L and W were the length and width of the shear band, d_i and d_e were the geometrical parameters of the hat-shaped specimen shown in Fig. 2.

The specimen impacted by SHPB had a circular cross-section and a narrow overlapping region concentrated the shear deformation. The etchant for TC16 alloy was 2.5 mL HF + 3 mL HNO_3 + 5 mL HCl + 91 mL H_2O.

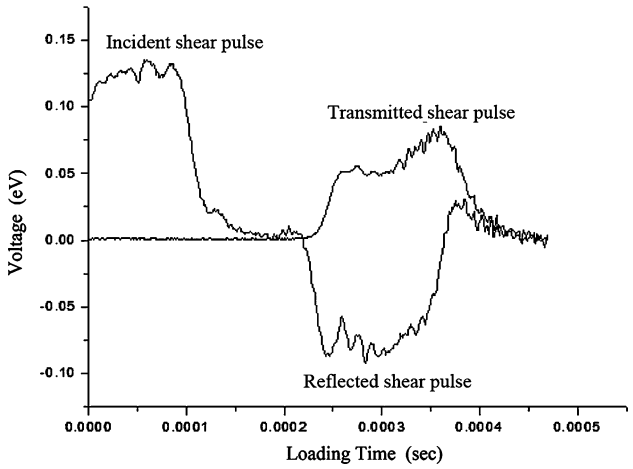

Fig. 1 Shear signals with the hat-shaped specimen attached between the bars

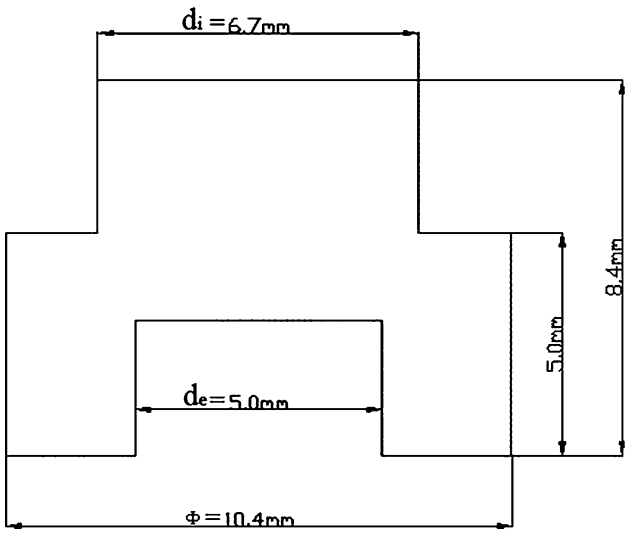

Fig. 2 Schematic diagram of the hat-shaped specimen

Investigations of Optical Microscope (OM) were performed with a POLYVAR-MET microscope. Microhardness tests were carried out with a microhardness instrument HMV-2 manufactured by SHIMADZU CORPORATION. The loading weight was 0.025 kg and the loading time was 60 s. Scanning electron microscopy (SEM) observations were carried out with a Sirion200 field emission scanning electron microscope operated at 10 kV. After hand grinding, the sample was reduced to a thickness of about 0.10 mm, and then the foils were perforated upon the shear band by electropolishing in a solution of 300 mL CH_3OH + 175 mL $C_4H_{10}O$ + 30 mL $HClO_4$ at 243 K. Finally, the foils for the transmission electron microscopy (TEM) were prepared by the sputter ion. TEM observations were carried out with a Tecanai G^2 20 transmission electron microscope operated at 200 kV.

Results and discussion

Flow stress–strain response

The strain rate within the shear band can be obtained from Eq. 2 and the time function of the reflected pulse strain is shown in Fig. 1. The starting time for ASB formation is just the instant when the strain rate reaches the first vibration peak [13, 14]. The shear deformation time for the specimen is about 122 μs, as shown in Fig. 3. The relation of the true flow stress and true strain in the ASB shown in Fig. 4 can be easily obtained by using Eqs. 1–4. It can be seen that three stages are proceeded during the shear deformation process. At first, the true flow stress increases with the true strain as (a → c) in Fig. 4 due to the strain hardening and the strain rate hardening, and the true flow stress reaches the maximum value at the first vibration peak. Next, the accumulation of the deformation energy is transformed into heat and increases the temperature when the deformation proceeds during (c → d) in Fig. 4, and the true flow stress fluctuations in a small area are a result of the rough balance of the thermal softening and the strain hardening and the strain rate hardening. Finally, the thermal softening is obviously larger than the hardening during (d → e) in Fig. 4, and the thermoviscoplastic instability occurs, that is, the ASB generates in the specimen.

Microstructure of the shear band

Figure 5 shows a montage of optical micrographs of ASB running through the gap of the specimen, and ASB is a "white" band with a width of about 13 μm. The "white" band in titanium alloy is often considered as a transformation band [1, 15, 16].

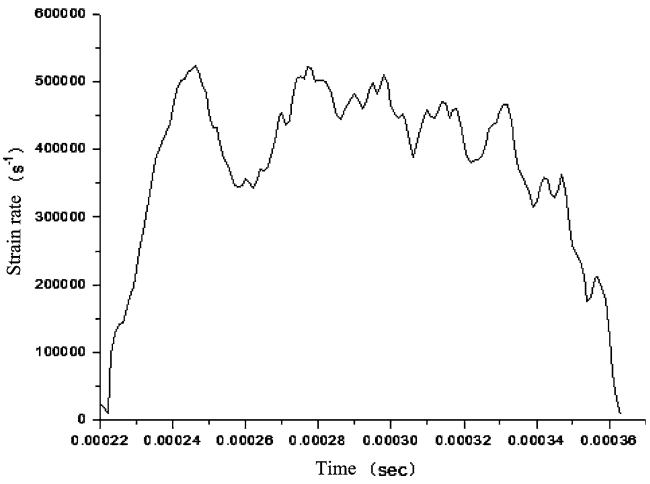

Fig. 3 Variation of the measured strain rate with the loading time

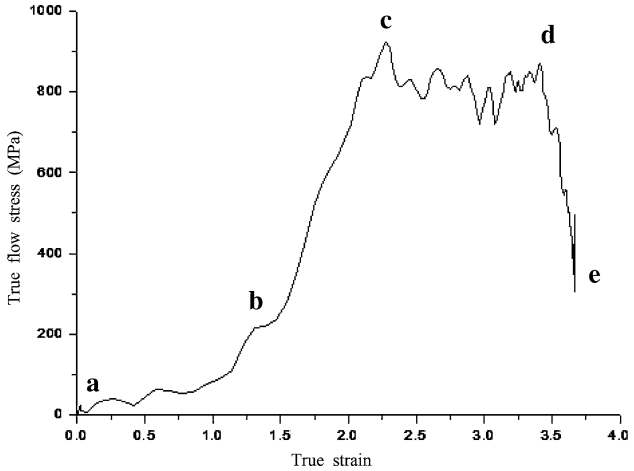

Fig. 4 The true flow stress versus true strain in the shear band during plastic deformation

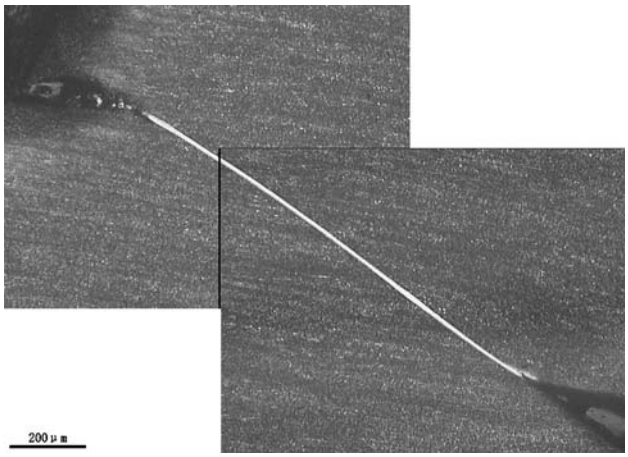

Fig. 5 A montage of optical micrographs of an ASB

Microhardness of ASB is tested at the middle part of the specimen, as shown in Fig. 6. We can see that the microhardness of the shear band is larger than that of the matrix due to the large deformation and very fine grains in the shear band [2, 3].

Figure 7 shows the scanning electron micrographs of ASB. It can be seen that the structure in the shear band is refined and elongated along the shear direction, and fiber structures exist in the transition zone between the center of ASB and matrix as a result of the strong shear deformation, and the pattern of the center of ASB obviously differs from that of the boundary of ASB and the structure is too dense to distinguish. Thus, there is obvious structure change from the boundary to the center of the shear band.

The grains in the boundary of ASB are shown in Fig. 8. It can be seen that the strong shear deformation upon the shear band leads to highly elongated grains in the boundary of the shear band and forms elongated cell structures of width about 0.2–0.5 μm with thick dislocation. The boundary of the shear band is often so narrow that the investigation of the elongated cell structures is difficult [3, 17, 18]. However, elongated cell structures are easily observed in this alloy as the fine grains of the matrix.

Figure 9 illustrates the microstructure in the center of the shear band. It consists of a number of equiaxed grains of diameters about 0.2 μm with low dislocation density, and these grains have a typical recrystallized character. SAD pattern taken from the center of the shear band shown in Fig. 9c indicates that the α-phase grains still exist in the region. From Fig. 9a and b, it can be seen that lots of plate structures are in the center of the shear band. There are two monocrystalline diffraction patterns of the plate structures in Fig. 9d because the sizes of the grains are less than those of the selected area. The indexed SAD pattern inserted in Fig. 9d reveals that the orthorhombic α''-phase martensite grains are generated in the shear band. The phase transformation $\beta \rightarrow \alpha''$ occurs in the ASB in TC16 alloy and causes the "white" band in Fig. 5.

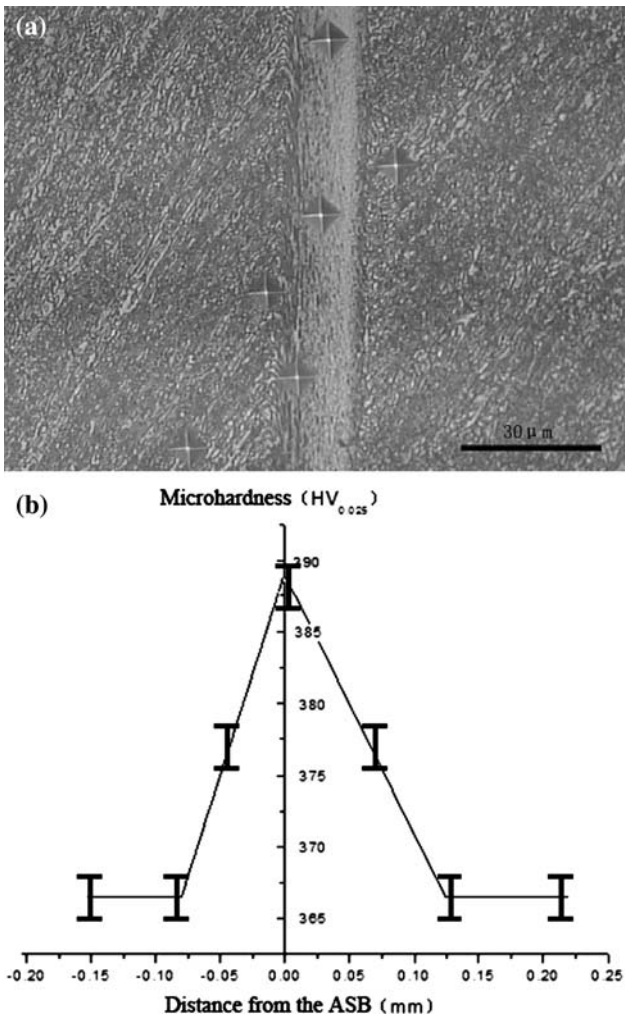

Fig. 6 Microhardness of the matrix and an ASB. (**a**) is the pattern of the microhardness, (**b**) is the microhardness versus position in the specimen. Note that the range of five tests in each position is marked in an error line

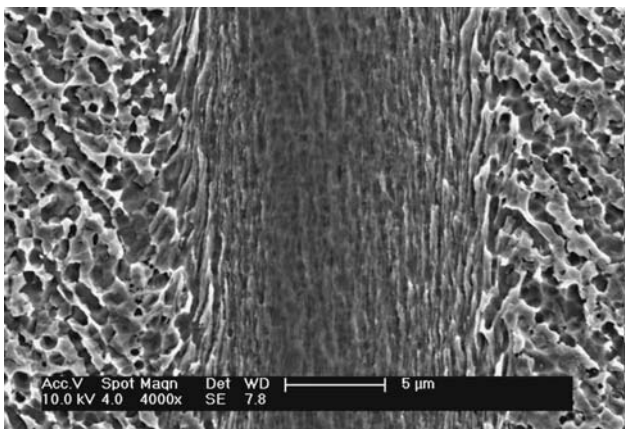

Fig. 7 SEM micrographs of ASB

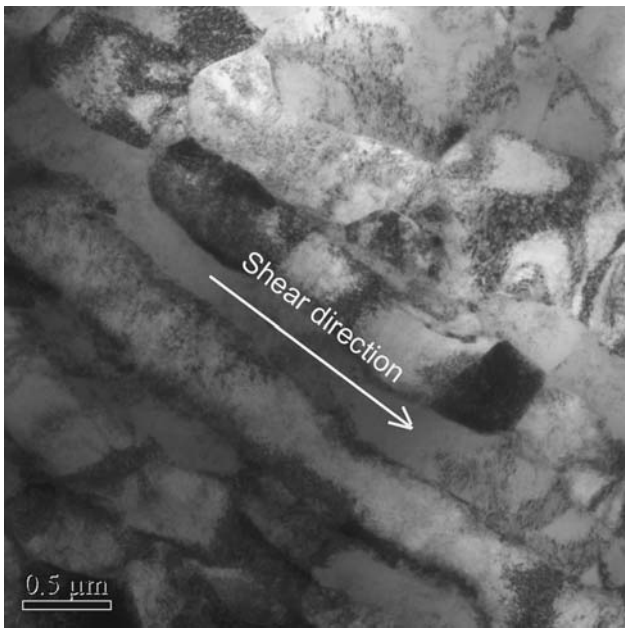

Fig. 8 The light field pattern of the microstructure in the boundary of the shear band

Estimate of adiabatic temperature rise and the formation of ASB

At high strain rates ($>10^3\ s^{-1}$), the deformation process is extremely fast and can be considered as an adiabatic process. The adiabatic temperature rise is an important parameter for the formation of an ASB and is calculated by the following equation [3, 19].

$$\Delta T = T - T_0 = \frac{\beta}{\rho C_V}\int_{\varepsilon_s}^{\varepsilon_e}\sigma\,\mathrm{d}\varepsilon \tag{5}$$

where T_0 is the ambient temperature, ρ is mass density, C_v is heat capacity, ε is the strain, σ is the stress, and β is the fraction of plastic energy converted to heat; commonly β is 0.9. For TC16 alloy, ρ is 4,647 kg/m^3, C_v is 470 J/(kg $\times$ K). Here, T_0 is 293 K.

By substituting the dynamic response data in the shear band during plastic deformation shown in Fig. 4 into Eq. 5, the adiabatic temperature rise can be estimated as follows.

$$\Delta T_{\max} = \frac{\beta}{\rho C_\upsilon}\int_{\varepsilon_s}^{\varepsilon_e}\sigma\,\mathrm{d}\varepsilon \doteq \frac{\beta}{\rho C_\upsilon}\sum S_{\mathrm{i}}\ (i = 1, 2, 3, \ldots) \tag{6}$$

where S_i is the deformation energy per unit area. The dynamic response data in the shear band shown in Fig. 4 can be divided into a large number of continuous blocks with strain increment $\Delta\varepsilon_i$, and the area of each block (S_i) can be calculated from the following expression:

$$S_i = \frac{\Delta\varepsilon_i \times \sigma_i + \sigma_{(i+1)}}{2}(i = 1,\ 2,\ 3,\ \ldots) \tag{7}$$

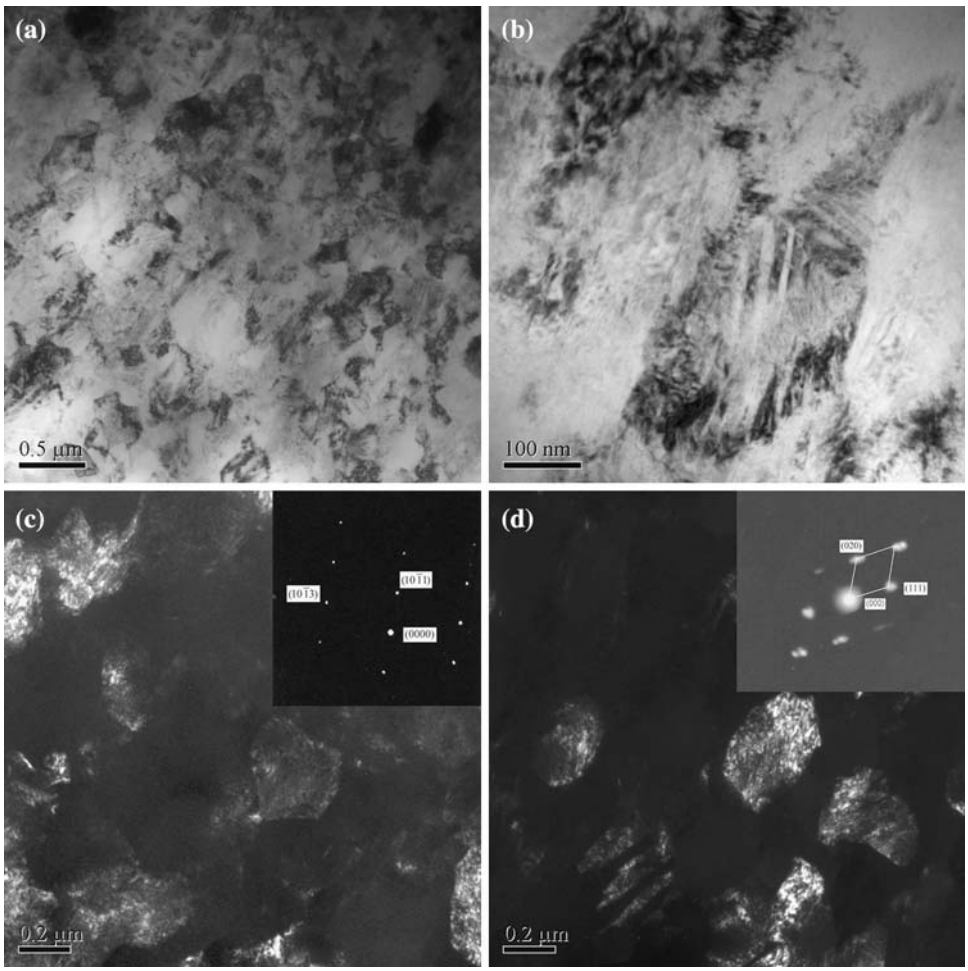

Fig. 9 TEM micrographs and SAD patterns showing the microstructure in the center of shear band. (**a**) and (**b**) are the light field pattern of the microstructure in the center of shear band, (**c**) and (**d**) are the dark field patterns and their corresponding SAD patterns of α-phase and α″-phase in (**a**), respectively

By substituting S_i into Eq. 6 the adiabatic temperature rise is calculated. Therefore, the relationships of the true strain to the temperature (here, $T = T_0 + \Delta T_{max}$) and of the time to the true strain and the temperature can be easily obtained by using Eqs. 3, 4, 6, and the measured data, as shown in Fig. 10. It can be seen that the maximum temperature within the shear band is about 1,069 K, as shown in Fig. 10a. Therefore, temperature in the shear band during the shear deformation is lower than the recrystallization point (1,093–1,143 K) of TC16 alloy at normal condition [5, 20]. However, the recrystallization occurs in the shear band shown in Fig. 9. Because the high dislocation density generated by adiabatic shear deformation increases the driven force for recrystallization, the temperature for dynamic recrystallization in material is lower than that for static recrystallization at normal condition.

The formation of an ASB in the TC16 alloy can be described by Fig. 10b as follows.

Both the deformation temperature and the true flow stress increase slowly with the true strain in the region (a → b) before the first vibration peak (at about 240 μs) in the time versus strain curve. It indicates that the material has already been loaded before the adiabatic shear deformation; however, deformation doesnot obviously occur due to the fine grains of the matrix.

At the first stage in the region (b → c), the deformation temperature increases with the increase of the true strain; however, the increment speed of the temperature decreases. And the inflectional point of the true strain emerges at about 252 μs at the point 'c' owning to the thermal softening weakens the strain and strain rate hardening, where the true strain is about 2.07 and temperature is about 505 K. In this stage, a large number of randomly distributed dislocations generated in the materials are deformed by the severe shear deformation, and the grains are obviously elongated.

At the next stage in the region (c → d), although the true strain increases slowly, the deformation temperature within the shear band increases fast when the deformation proceeds and reaches the first peak at about 341 μs at the point 'd', where the true strain is about 3.56 and temperature is about 1,048 K. During this process, a large number

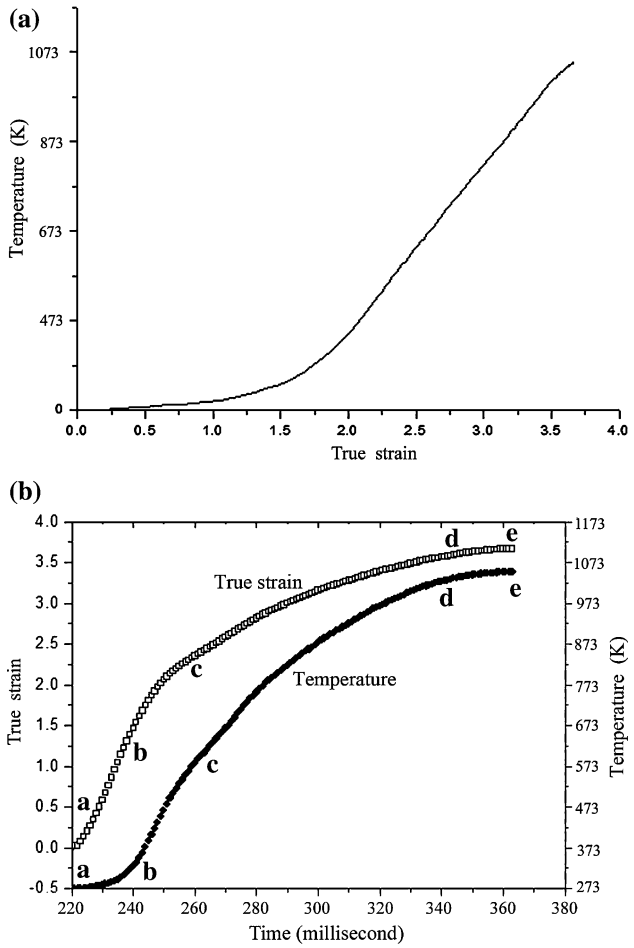

Fig. 10 (**a**) is the relationship of the true strain to the temperature and (**b**) is the relationship of the time to the true strain and the temperature

of the deformation works generate and provide the needed energy for the microstructure evolution of the ASB. Kinetics calculation of the dynamic recrystallization indicated that this stage provided the stored energy and the subgrains before the occurrence of the recrystallization [20]. Elongated subgrains are plastically deformed leading to break up and form approximately equiaxed subgrains.

At the third stage in the region (d → e), the true strain increases little and the temperature within the shear band reaches the maximum value (about 1,069 K) and the thermoviscoplastic instability occurs at about 362 μs and the adiabatic shear deformation is completed. Kinetics calculation of the microstructural evolution in ASB in many metals [19, 21, 22] indicated that the fine equiaxed grains could be formed by the rotational dynamic recrystallization mechanism and they had not undergone significant growth by grain boundary migration during cooling. Thus, during the last stage and the next cooling stage, the new fine equiaxed grains form in manner of the grain-boundary rotation about 30°; at the same time, the phase transformation occurs and the microstructural evolution in the ASB is completed.

Conclusions

Dynamic testing of Ti-3Al-5Mo-4.5V (TC16) alloy was carried out in an SHPB at ambient temperature. ASB in TC16 alloy is a "white" band with a width of about 13 μm. The grains in the boundary of the shear band are highly elongated along the shear direction and form the elongated cell structures of width about 0.2–0.5 μm with thick dislocation. The fine equiaxed grains with α-phase and α″-phase coexist in the shear band. The phase transformation occurring in the shear band causes the "white" band. By substituting the dynamic response data in the shear band during plastic deformation into the expression of the adiabatic temperature rise calculation, the maximum temperature within ASB is about 1,069 K that is above the phase transformation temperature. Within the deformation time (about 122 μs), the grains can carry out the following processes: randomly distributed dislocations are generated, the grains are obviously elongated, elongated subgrains break up and form approximately equiaxed subgrains, subgrains rotate, and finally form recrystallized grains.

Acknowledgements This work was financially supported by the National Nature Science Foundation of China, No. 50471059 and No. 50671121.

References

1. Bai YL (1990) Res Mech 31:133
2. Meyers MA, Park HR (1986) Acta Metall 34:2493
3. Yang Y, Zhang XM, Li ZH (1996) Acta Mater 44:561
4. Xue Q, Meyers MA, Nesterenko VF (2002) Acta Mater 50:575
5. Bophcoba EA (1986) Metallography of titanium alloy. National Defence Industry Press, Beijing, p 326
6. Zong YY, Shan DB, Lu Y (2006) J Mater sci 41:3753. doi:10.1007/s10853-006-2658-z
7. Hung F-Y, Lui T-S (2005) J Mater Sci 40:3683. doi: 10.1007/s10853-005-3310-z
8. Wang R, Yang GY, Wu BX, Fu BW, Zhan YC, Zhang YH (1991) Proceedings of SPIE—The International Society for Optical Engineering, vol 1519, p 146
9. Rusakov GM, Litvinov AV (2002) Fiz Met Metalloved 93:17
10. Meyer LW, Manwarig S (1986) In: Murr LE, Staudhammer KP, Meyers MA (eds) Metallurgical applications of shock-wave and high-strain—Rate Phenomena. Marcel Dekker, New York, p 657
11. Andrade U, Meyers MA (1994) Acta Mater 42:3183
12. Culver RS (1973) In: Rohde RW, Butcher BM, Holland JR (eds) Metallurgical effects at high strain rates. Plenum Press, New York, p 519
13. Hines JA, Vecchio KS (1997) Acta Metall Mater 45:635
14. Li Q, Xu YB, Lai ZH, Shen LT, Bai YL (2000) Mater Sci Eng A276:250
15. Timothy SP, Hutchings IM (1985) Acta Metall 33:667
16. Bayoumi AE, Xie JQ (1995) Mater Sci Eng A190:173

17. Grebe HA, Pak HR (1985) Metall Trans 16A:761
18. Meyers MA, Subhash G, Kad BK, Prasad L (1994) Mech Mater 17:175
19. Meyers MA, Xu YB, Xue Q et al (2003) Acta Mater 51:1307
20. Zhang XY, Zhao YQ, Bai CG (2005) Titanium alloy and its application. Chemical Industry Press, Beijing, p 86
21. Yang Y, Wang BF (2006) J Mater Sci 41:7387. doi: 10.1007/s10853-006-0811-3
22. Kad BK, Gebert J-M, Perez-Prado MT, Kassner ME, Meyers MA (2006) Acta Mater 54:4111